Eur. J. Mech. B - Fluids 20 (2001) 187–204

S0997-7546(00)01112-2/FLA

Transient boundary-layer heat transfer from a flat plate subjected to a sudden change in heat flux

Simon D. Harris [a], Derek B. Ingham [b], Ioan Pop [c,*]

[a] *Rock Deformation Research, School of Earth Sciences, University of Leeds, Leeds LS2 9JT, UK ;* [b] *Department of Applied Mathematics, University of Leeds, Leeds LS2 9JT, UK ;* [c] *Faculty of Mathematics, University of Cluj, R–3400 Cluj, CP 253, Romania*

(Received 20 April 2000; revised 4 September 2000; accepted 12 September 2000)

Abstract – We examine the transient forced convection heat transfer from a fixed, semi-infinite, flat plate situated in a fluid which, at large distances, is moving with a constant velocity parallel to the plate. Both the fluid and the plate are initially at a constant temperature and the transients are initiated when the zero heat flux at the plate is suddenly changed to a constant value. The thermal boundary-layer equations are solved using numerical techniques to extend a series which is valid for small times and describe fully the development from the initial unsteady state solution (small times) to the ultimate steady state solution (large time). © 2001 Éditions scientifiques et médicales Elsevier SAS

transient flow / boundary-layer / heat flux / analytical and numerical methods

Nomenclature

f	non-dimensional, reduced streamfunction
F	non-dimensional streamfunction f expressed in terms of ξ
G	non-dimensional, transformed variable, $= \frac{1}{2}(\frac{\sigma}{\tau})^{1/2}\theta$
k	thermal conductivity of the fluid
q_w	constant plate heat flux applied for $\tau \geqslant 0$
s	non-dimensional variable, $= (\frac{\lambda\sigma}{\alpha^2})^{1/3}(\alpha\zeta - 1)$
t	time
T	fluid temperature
$\mathcal{T}$	dominant τ dependence in the inner solution at large times
T_∞	ambient fluid temperature
U_∞	constant velocity of the fluid at a large distance from the plate
u, v	fluid velocity components along x- and y-directions, respectively
x, y	Cartesian coordinates along the plate and normal to it, respectively
$\mathcal{X}$	function introduced for the inner solution at large times

* Correspondence and reprints.
E-mail address: popi@math.ubbcluj.ro (I. Pop).

Greek symbols

α	constant, $= f''(0)$
ζ	variable used for the inner solution at large times, $= \tau\eta$
η	non-dimensional similarity variable, $= y(\frac{U_\infty}{\nu x})^{1/2}$
θ	non-dimensional, reduced temperature function, $= \frac{T-T_\infty}{\frac{q_w}{k}(\frac{\nu x}{U_\infty})^{1/2}}$
ν	kinematic viscosity
ξ	non-dimensional transformed variable, $= \frac{1}{2}\eta(\frac{\sigma}{\tau})^{1/2}$
σ	Prandtl number
τ	non-dimensional time, $= U_\infty \frac{t}{x}$
ψ	streamfunction

1. Introduction

The fundamental problem of the transient momentum (velocity) and thermal boundary layers past heated surfaces has long been the subject of many investigators. An extensive amount of literature on this topic may be found in the monographs and review articles by Riley [1,2], Shen [3], Telionis [4,5] and Pop [6]. The problem of describing the transition from the initial unsteady state solution (small time) to the ultimate steady state solution (large time) has proved to be a difficult one. However, a great part of the published work refers mainly to the momentum boundary-layer. In many engineering applications it is important to include and also derive a number of pivotal results for the heat transfer effects in unsteady boundary-layer flows. Almost all previous investigations, see Riley [7], Chao and Cheema [8], Dennis [9], Van Dyke [10], Watkins [11] and Jeng et al. [12], attack the problem of the transient heat transfer initiated by a step change in the temperature of the plate over which a fluid is passing. Additionally, in all these papers, the plate boundary condition used did not vary with position on the plate, and the velocity field was steady.

Van Dyke [10] was the first who has studied the growth of the thermal boundary-layer produced by a sudden change in the temperature of a semi-infinite flat plate in a uniform stream with an established (steady) momentum boundary-layer using a numerical procedure to extend a perturbation series in powers of small time τ (non-dimensional). However, Van Dyke [10] has not used his small time solution ($\tau < 1$) to investigate the transition from the initial unsteady to the final state state solution as $\tau \to \infty$.

In many practical and experimental circumstances the thermal boundary-layer is generated adjacent to surfaces which are dissipating heat at a prescribed rate. Therefore, the purpose of this paper is to provide a better model of the physical situations which occur in practice and we study the transient heat transfer in the boundary-layer flow over a flat plate whose temperature is suddenly changed when a constant surface heat flux q_w is imposed at the plate surface. We present accurate, numerical solutions of the governing equation using an extended series expansion in powers of small time, as suggested by Van Dyke [10] in combination with the Shanks transformation technique, see Shanks [13], to extend this small time solution to a solution which is valid for large time. Numerical results are presented in tabular and graphical form for some values of the Prandtl number. It is shown that the series solution can be used to provide an accurate representation of the transient behaviour over an initial time period but that the steady state solution, obtained from the direct numerical solution of the steady thermal boundary-layer equation, cannot be reached by this approach.

A sequence of numerical procedures are therefore employed to provide a complete numerical solution of the full thermal boundary-layer equation and enable a characterisation of the general transients arising from the

imposition of a constant heat flux on the plate surface. The very detailed numerical solution presented for the whole transient from $\tau = 0$ to the steady state $\tau \to \infty$ consists of a modification of the step-by-step method proposed by Merkin [14] in combination with a finite-difference method similar to that devised by Dennis [15], which has been used on a range of problems, see, for example, Walker and Dennis [16] and Harris et al. [17–20]. The effect of the value of the Prandtl number, σ, on the temperature field is investigated through a study of the particular cases $\sigma = 0.72$ (air) and 6.7 (water).

2. Governing equations

Consider the forced convection flow past a fixed, semi-infinite, flat plate situated in a fluid of uniform temperature for $t < 0$. At large distances from the plate surface, the fluid is moving with a constant velocity U_∞ parallel to the plate. It is assumed that at $t = 0$ a steady velocity boundary-layer has already been established and it is described by the equations

$$\frac{\partial u}{\partial x} + \frac{\partial v}{\partial y} = 0, \tag{1}$$

$$u\frac{\partial u}{\partial x} + v\frac{\partial u}{\partial y} = \nu\frac{\partial^2 u}{\partial y^2}, \tag{2}$$

where x and y are the Cartesian coordinates measured, respectively, along and normal to the plate, u and v are the velocity components along the x and y axes and ν is the kinematic viscosity. The boundary conditions to be applied to equations (1) and (2) are given by

$$\begin{aligned} &u = 0, \qquad v = 0 \quad \text{on } y = 0,\ x > 0, \\ &u = U_\infty \quad \text{on } x = 0,\ y > 0, \\ &u \to U_\infty \quad \text{as } y \to \infty \end{aligned} \tag{3}$$

for all times t.

Further, it is assumed that at $t \leqslant 0$ both the plate and fluid are at the same uniform temperature T_∞, so that there is zero heat flux at the plate. Then, at $t = 0$, the zero heat flux at the plate is suddenly changed by imposing a constant heat flux q_w, thereby setting up a time dependent thermal boundary-layer. The growth of the thermal boundary-layer may be described by the equation

$$\frac{\partial T}{\partial t} + u\frac{\partial T}{\partial x} + v\frac{\partial T}{\partial y} = \frac{\nu}{\sigma}\frac{\partial^2 T}{\partial y^2}, \tag{4}$$

where T is the fluid temperature and σ is the Prandtl number. Here we have tacitly assumed that the Eckert number is very small, so that the viscous dissipation effects can be neglected. The initial and boundary conditions for equation (4) are given by

$$\begin{aligned} &T = T_\infty \quad \text{for all } x > 0,\ y > 0 && \text{for } t \leqslant 0, \\ &\left.\begin{aligned} &T = T_\infty \quad \text{on } x = 0,\ y > 0, \\ &\frac{\partial T}{\partial y} = -\frac{q_w}{k} \quad \text{on } y = 0,\ x > 0, \\ &T \to T_\infty \quad \text{as } y \to \infty \end{aligned}\right\} && \text{for } t > 0, \end{aligned} \tag{5}$$

where k is the thermal conductivity of the fluid.

The solution of equations (1) and (2) under the boundary conditions (3) is defined by

$$u = U_\infty f'(\eta), \qquad v = \frac{1}{2}\left(\frac{U_\infty \nu}{x}\right)^{1/2}\left[\eta f'(\eta) - f(\eta)\right], \tag{6}$$

where primes denote differentiation with respect to the non-dimensional similarity variable η, which is defined as

$$\eta = y\left(\frac{U_\infty}{\nu x}\right)^{1/2}. \tag{7}$$

The non-dimensional, reduced streamfunction $f(\eta)$ is defined according to

$$\psi = (U_\infty \nu x)^{1/2} f(\eta), \tag{8}$$

where the streamfunction ψ is defined in the usual way, namely $u = \partial\psi/\partial y$ and $v = -\partial\psi/\partial x$. The transient solution for the temperature function T is obtained by solving equation (4), subject to the boundary conditions (5), through the introduction of a non-dimensional, reduced temperature function $\theta(\eta, \tau)$, where

$$T = T_\infty + \left(\frac{\nu x}{U_\infty}\right)^{1/2}\frac{q_w}{k}\theta(\eta, \tau), \quad \tau = U_\infty \frac{t}{x} \tag{9}$$

and τ is the non-dimensional time.

The equations governing the solutions for the functions $f(\eta)$ and $\theta(\eta, \tau)$ can be obtained by substituting expressions (7) to (9) into equations (1), (2) and (4). It is found that these functions satisfy the pair of equations

$$f''' + \frac{1}{2} f f'' = 0, \tag{10}$$

$$\frac{1}{\sigma}\frac{\partial^2\theta}{\partial\eta^2} + \frac{1}{2} f \frac{\partial\theta}{\partial\eta} - \frac{1}{2} f'\theta = (1 - \tau f')\frac{\partial\theta}{\partial\tau} \tag{11}$$

which must be solved for $\tau > 0$, subject to the initial and boundary conditions

$$\left.\begin{array}{ll} \theta = 0 \quad \text{for } \eta \geqslant 0 & \\ f(0) = 0, \qquad f'(0) = 0, \qquad \dfrac{\partial\theta}{\partial\eta}(0, \tau) = -1, & \\ f' \to 1, \qquad \theta \to 0 \quad \text{as } \eta \to \infty & \end{array}\right\} \begin{array}{l} \text{at } \tau = 0, \\ \\ \text{for } \tau > 0. \end{array} \tag{12}$$

It is worth noting that equation (10) is the well-known Blasius equation, whilst equation (11) describes the transient flow in the present problem and it has not previously been solved. Equation (11) is also the appropriate form of the energy equation for studying the final decay to steady state.

A common starting point for the discussion of transient problems is to examine their behaviour for small times. A study of this transient process then reveals some of the basic features of the full boundary-layer equations and also provides a framework against which to develop the general transient process. This is where we begin our investigation.

3. Small time solution of the energy equation, $\tau \ll 1$

In the early development of the flow there exists an inner thermal boundary-layer for $\tau \ll 1$, which is described by equation (11). Outside this layer, the initial state is maintained so that the fluid temperature has the uniform value T_∞ or, in non-dimensional form, $\theta = 0$. Since the appropriate length scale for small times is the diffusion scale, $\tau^{1/2}$, we use the new independent variables ξ and τ and introduce the following definitions:

$$\xi = \frac{1}{2}\eta\left(\frac{\sigma}{\tau}\right)^{1/2}, \qquad \theta(\eta,\tau) = 2\left(\frac{\tau}{\sigma}\right)^{1/2} G(\xi,\tau). \tag{13}$$

Substituting these variables into equation (11) yields

$$\frac{\partial^2 G}{\partial \xi^2} + \left[(\sigma\tau)^{1/2}(F - \xi F') + 2\xi\right]\frac{\partial G}{\partial \xi} - 2G = 4\tau\left[1 - \frac{1}{2}(\sigma\tau)^{1/2}F'\right]\frac{\partial G}{\partial \tau}, \tag{14}$$

where $F(\xi) = f(\eta)|_{\eta=2\xi(\frac{\tau}{\sigma})^{1/2}}$ and primes denote differentiation with respect to ξ. The appropriate boundary conditions for equation (14) are

$$\left.\begin{aligned} &\frac{\partial G}{\partial \xi}(0,\tau) = -1, \\ &G \to 0 \quad \text{as } \xi \to \infty \end{aligned}\right\} \quad \text{for } \tau > 0. \tag{15}$$

The solution of equation (14) for $\tau \ll 1$ within the thin, growing inner thermal layer is achieved by replacing the velocity function $F(\xi) = f(\eta)|_{\eta=2\xi(\frac{\tau}{\sigma})^{1/2}}$ with its series expansion near to the plate. The solution of equation (10) for the Blasius function at small values of η can be approximated by Weyl's expansion, see Rosenhead [21], as follows:

$$f(\eta) = \sum_{n=0}^{\infty} \alpha^{n+1} D_n \left(-\frac{1}{2}\eta\right)^{2+3n}, \tag{16}$$

where $\alpha \equiv f''(0)$ and the coefficients D_n satisfy the recurrence relation

$$3n(3n+1)(3n+2)D_n = \sum_{i=0}^{n-1}(3i+1)(3i+2)D_i D_{n-i-1} \tag{17}$$

with $D_0 = 2$. The value of α is determined by solving equation (10) using the NAG routine D02HAF, an algorithm which solves two-point boundary-value problems for systems of first-order, ordinary differential equations using a Runge–Kutta–Merson method and a Newton iteration in a shooting and matching technique. Thus, we find $\alpha = 0.3320573$.

Further, it can be verified that the solution of equation (14) for the temperature function G at small values of τ ($\ll 1$) has the following form, see Riley [7]:

$$G(\xi,\tau) = \sum_{n=0}^{\infty} \tau^{3/2n} \mathcal{G}_n(\xi). \tag{18}$$

Substitution of the series (18) into equation (14) leads to the following sets of ordinary differential equations:

$$\mathcal{G}_0'' + 2\xi\mathcal{G}_0' - 2\mathcal{G}_0 = 0, \tag{19}$$

$$\mathcal{G}_1'' + 2\xi\mathcal{G}_1' - 8\mathcal{G}_1 = 2\frac{\alpha}{\sigma^{1/2}}\xi^2\mathcal{G}_0', \tag{20}$$

$$\begin{aligned}\mathcal{G}_n'' + 2\xi\mathcal{G}_n' - 2(3n+1)\mathcal{G}_n = {}& \frac{\alpha}{\sigma^{1/2}}\xi^2\sum_{m=0}^{n-1}(3m+1)D_m(-\alpha)^m\sigma^{-3m/2}\xi^{3m}\mathcal{G}_{n-m-1}' \\ & - 3\frac{\alpha}{\sigma^{1/2}}\xi\sum_{m=0}^{n-2}(n-m-1)(3m+2)D_m(-\alpha)^m\sigma^{-3m/2}\xi^{3m}\mathcal{G}_{n-m-1}\end{aligned} \tag{21}$$

for $n \geqslant 2$, which must be solved subject to

$$\mathcal{G}_0(\infty) = 0, \qquad \mathcal{G}_n(\infty) = 0, \qquad \mathcal{G}_0'(0) = -1, \qquad \mathcal{G}_n'(0) = 0 \tag{22}$$

for $n \geqslant 1$. Primes now denote differentiation with respect to ξ. It should be noted that equations (19) to (21) have a form similar to those obtained by Riley [7], but the boundary conditions are different.

The solutions of equations (19) to (21), together with the boundary conditions (22), for $\mathcal{G}_0$, $\mathcal{G}_1$ and $\mathcal{G}_2$ are given by

$$\mathcal{G}_0(\xi) = -\xi\,\mathrm{erfc}\,\xi + \frac{1}{\pi^{1/2}}\mathrm{e}^{-\xi^2}, \tag{23}$$

$$\mathcal{G}_1(\xi) = \frac{\alpha}{\sigma^{1/2}}\left[\left(\frac{1}{64} + \frac{1}{16}\xi^2 - \frac{7}{48}\xi^4\right)\mathrm{erfc}\,\xi + \frac{1}{\pi^{1/2}}\left(\frac{1}{32}\xi + \frac{7}{48}\xi^3\right)\mathrm{e}^{-\xi^2}\right], \tag{24}$$

$$\begin{aligned}\mathcal{G}_2(\xi) = {}& \frac{\alpha^2}{\sigma}\left\{\left[-\frac{1}{32}\xi^3 - \frac{3}{80}\xi^5 + \left(\frac{13}{1260} + \frac{4}{315\sigma}\right)\xi^7\right]\mathrm{erfc}\,\xi\right. \\ & + \frac{1}{\pi^{1/2}}\left[\frac{67}{6720} - \frac{1}{840\sigma} + \left(\frac{67}{840} - \frac{1}{105\sigma}\right)\xi^2 + \left(\frac{71}{1008} - \frac{1}{63\sigma}\right)\xi^4\right. \\ & \left.\left. + \left(-\frac{13}{1260} - \frac{4}{315\sigma}\right)\xi^6\right]\mathrm{e}^{-\xi^2}\right\},\end{aligned} \tag{25}$$

where $\mathrm{erfc}\,\xi = \frac{2}{\pi^{1/2}}\int_\xi^\infty \mathrm{e}^{-s^2}\,\mathrm{d}s$ is the complementary error function.

The terms $\mathcal{G}_n$ in the series expansion for $G(\xi,\tau)$, valid for small values of τ, can be obtained using a computer extension technique, namely that described by Van Dyke [10]. It can be verified by induction that the solution of equation (21) subject to the boundary conditions (22) has the following form:

$$\begin{aligned}\mathcal{G}_n = \alpha^n\left[A_{n,0}\left\{\begin{array}{c}\mathrm{e}^{-\xi^2}\\ \mathrm{erfc}\,\xi\end{array}\right\} + A_{n,1}\xi\left\{\begin{array}{c}\mathrm{erfc}\,\xi\\ \mathrm{e}^{-\xi^2}\end{array}\right\} + A_{n,2}\xi^2\left\{\begin{array}{c}\mathrm{e}^{-\xi^2}\\ \mathrm{erfc}\,\xi\end{array}\right\} + \cdots\right. \\ \left. + A_{n,3n}\xi^{3n}\mathrm{e}^{-\xi^2} + A_{n,3n+1}\xi^{3n+1}\mathrm{erfc}\,\xi\right] \quad \text{for} \left\{\begin{array}{c}n \text{ even}\\ n \text{ odd}\end{array}\right\},\end{aligned} \tag{26}$$

where

$$A_{n,1} = \begin{cases} 0 & \text{for } n \text{ even},\\ \dfrac{2}{\pi^{1/2}}A_{n,0} & \text{for } n \text{ odd}.\end{cases} \tag{27}$$

Substituting the solution (26) into equation (21) and equating coefficients of like powers of ξ for terms in both $e^{-\xi^2}$ and $\operatorname{erfc}\xi$ yields a tri-diagonal system of $3n+2$ simultaneous equations for the $3n+2$ unknowns $A_{n,0},\ldots,A_{n,3n+1}$ which can be inverted using the Thomas algorithm in order to advance the solution to the next term in the series (18).

4. Large time solution of the energy equation, $\tau \gg 1$

For large times we consider the energy equation in the form (11). The steady state solution $\theta_0(\eta)$ is defined by the following ordinary differential system:

$$\begin{aligned} &\frac{1}{\sigma}\theta_0'' + \frac{1}{2}f\theta_0' - \frac{1}{2}f'\theta_0 = 0, \\ &\theta_0'(0) = -1, \qquad \theta_0(\infty) = 0, \end{aligned} \tag{28}$$

where primes again denote differentiation with respect to η, which is obtained by neglecting the time-dependent term in equation (11) and imposing the appropriate boundary conditions (12). For each value of η, the steady state solution is approached gradually as $\tau \to \infty$ and thus we seek a perturbation of the steady state solution in the form

$$\theta(\eta,\tau) = \theta_0(\eta) + \theta_1(\eta,\tau) \tag{29}$$

to investigate how the steady state is realised at large values of τ. Then, from equations (11) and (12), the function $\theta_1(\eta,\tau)$ satisfies

$$\frac{1}{\sigma}\frac{\partial^2\theta_1}{\partial\eta^2} + \frac{1}{2}f\frac{\partial\theta_1}{\partial\eta} - \frac{1}{2}f'\theta_1 = (1-\tau f')\frac{\partial\theta_1}{\partial\tau} \tag{30}$$

which must be solved subject to the boundary conditions

$$\frac{\partial\theta_1}{\partial\eta}(0,\tau) = 0, \qquad \theta_1(\infty,\tau) = 0 \tag{31}$$

and this forms an eigenvalue problem for the function $\theta_1(\eta,\tau)$.

The approach which we follow to determine the behaviour of $\theta_1(\eta,\tau)$ at large times τ is that adapted by Riley [7], being initially an extension of the work of Stewartson [22] carried out by Watson (see the appendix to the paper by Dennis [15]). In the final decay to the steady state, departures from the steady state solution are concentrated near to the plate. Therefore, for large τ we seek an inner solution to the governing equation (30) in the form

$$\theta_1(\eta,\tau) = \mathcal{T}(\tau)\mathcal{X}(\zeta,\tau), \tag{32}$$

where $\zeta = \tau\eta$ is the variable introduced by Stewartson [22]. As in the case of the associated problem of Riley [7], it may be verified that

$$\mathcal{T}(\tau) = \tau^c \exp\left(-\frac{1}{3}\lambda\tau^3\right), \tag{33}$$

where c and λ are constants, and

$$\mathcal{X}(\zeta,\tau) = \mathcal{X}_0(\zeta) + \tau^{-3}\mathcal{X}_3(\zeta) + \tau^{-6}\mathcal{X}_6(\zeta) + \cdots \tag{34}$$

is the form of the solution for $\mathcal{X}$ and no other powers of τ^{-1} are required in equation (34). Introducing expression (32) and the small η solution (16) for $f(\eta)$, namely

$$f(\eta) = \frac{1}{2}\alpha\eta^2 - \frac{1}{240}\alpha^2\eta^5 + \mathrm{O}(\eta^8) \tag{35}$$

written in terms of ζ, τ, into the governing equation (30) for θ_1 we obtain

$$\frac{1}{\sigma}\mathcal{X}_0'' + \lambda(1-\alpha\zeta)\mathcal{X}_0 = 0, \tag{36}$$

$$\frac{1}{\sigma}\mathcal{X}_3'' + \lambda(1-\alpha\zeta)\mathcal{X}_3 = \left[\zeta(1-\alpha\zeta) - \frac{1}{4}\alpha\zeta^2\right]\mathcal{X}_0' + \left[c(1-\alpha\zeta) + \frac{1}{2}\alpha\zeta - \frac{1}{48}\lambda\alpha^2\zeta^4\right]\mathcal{X}_0 \tag{37}$$

by equating coefficients of powers of τ, where primes denote differentiation with respect to ζ. These equations for $\mathcal{X}_0$ and $\mathcal{X}_3$ must be solved subject to the boundary conditions

$$\mathcal{X}_0'(0) = 0, \qquad \mathcal{X}_3'(0) = 0, \qquad \mathcal{X}_0(\infty) = 0, \qquad \mathcal{X}_3(\infty) = 0. \tag{38}$$

To determine $\mathcal{X}_0$ and $\mathcal{X}_3$ it is convenient to define the new variable s according to

$$s = \left(\frac{\lambda\sigma}{\alpha^2}\right)^{1/3}(\alpha\zeta - 1) \tag{39}$$

and write $\bar{\mathcal{X}}_j(s)$ to be the resulting form of $\mathcal{X}_j(\zeta)$, for each $j = 0, 3, 6, \ldots$. The governing equation (36) and the associated boundary conditions (38) for $\bar{\mathcal{X}}_0(s)$ can then be written as

$$\bar{\mathcal{X}}_0'' - s\bar{\mathcal{X}}_0 = 0, \qquad \bar{\mathcal{X}}_0'\left[-\left(\frac{\lambda\sigma}{\alpha^2}\right)^{1/3}\right] = 0, \qquad \bar{\mathcal{X}}_0(\infty) = 0. \tag{40}$$

The governing equation for $\bar{\mathcal{X}}_0$ and the boundary condition as $s \to \infty$ are satisfied by the function $\bar{\mathcal{X}}_0(s) = C_0\mathrm{Ai}(s)$, where $\mathrm{Ai}(s)$ denotes the Airy function (see Bender and Orszag [23]) and C_0 is an arbitrary constant. The remaining boundary condition at $\zeta = 0$ provides an eigenvalue problem for λ. For $s > 0$, $\mathrm{Ai}'(s)$ has no zeros for finite s but, for $s < 0$, $\mathrm{Ai}'(s)$ has an infinite number of zeros at $s = -s_n$ with

$$\mathrm{Ai}'(-s_n) = 0, \qquad \mathrm{Ai}(-s_n) \neq 0 \tag{41}$$

for $n = 1, 2, 3, \ldots$. Only the first of these solutions is expected to be significant, leading to the largest contribution to $\mathcal{T}(\tau)$ in equation (33) at large values of τ. Then, $s_1 = 1.018793$ and the corresponding value of λ is

$$\lambda_1 = \frac{s_1^3\alpha^2}{\sigma} = 0.116596\sigma^{-1}. \tag{42}$$

Similarly, the governing equation and the boundary condition as $s \to \infty$ for $\bar{\mathcal{X}}_3(s)$ can be solved to give

$$\bar{\mathcal{X}}_3(s) = \tilde{\mathcal{X}}_3(s) + C_3\mathrm{Ai}(s), \tag{43}$$

where the particular solution $\tilde{\mathcal{X}}_3(s)$ for $\bar{\mathcal{X}}_3(s)$ is given by

$$\tilde{\mathcal{X}}_3(s) = -\frac{C_0}{4\alpha^2}\left\{\frac{1}{2}\frac{s}{s_1}\mathrm{Ai}(s)\left[\left(\sigma-\frac{1}{5}\right)+\left(3\sigma-\frac{1}{7}\right)\frac{s}{s_1}+\frac{1}{3}\left(5\sigma-\frac{1}{9}\right)\left(\frac{s}{s_1}\right)^2\right]\right.$$
$$+\frac{1}{s_1^2}\mathrm{Ai}'(s)\left[\left(\frac{1}{7}-5\sigma\right)+\frac{1}{3}\left(\frac{1}{9}+\left(4c-7\right)\sigma\right)\frac{s}{s_1}\right.$$
$$\left.\left.+s_1^3\left(\frac{1}{12}+\frac{1}{9}\frac{s}{s_1}+\frac{1}{10}\left(\frac{s}{s_1}\right)^2+\frac{1}{21}\left(\frac{s}{s_1}\right)^3+\frac{1}{108}\left(\frac{s}{s_1}\right)^4\right)\right]\right\}. \tag{44}$$

The constant C_3 is determined when the solution for $\mathcal{X}_6(\zeta)$ is investigated and is non-zero. The remaining boundary condition $\bar{\mathcal{X}}_3(-s_1)=0$ determines the value of c appropriate to the dominant root $s=-s_1$ to be

$$c_1 = \frac{4}{315\sigma}(7+2s_1^3)-2 = 0.115745\sigma^{-1}-2. \tag{45}$$

As $\tau\to\infty$ we have therefore obtained the following dominant terms for θ_1:

$$\theta_1(\eta,\tau) = C_0\tau^{c_1}\exp\left(-\frac{1}{3}\frac{s_1^3\alpha^2}{\sigma}\tau^3\right)\left\{\mathrm{Ai}\left[s_1(\alpha\tau\eta-1)\right]+\mathrm{O}\left(\tau^{-3}\right)\right\}, \tag{46}$$

where the constant C_0 will depend, in some manner, upon the initial growth of the thermal boundary-layer.

5. Numerical solutions

Initially the transient effects due to the imposition of a constant surface heat flux at the flat plate are confined to a thin fluid region near to the surface and are described by the small time solution developed in section 3. These effects continue to penetrate outwards through the initial boundary-layer and eventually evolve into a new steady state flow. In order to match these small and large time solutions we now develop a numerical solution of the thermal boundary-layer equation (4) by initially using the formulation (14) in terms of ξ, τ and subsequently the governing equation (11) in terms of η, τ, where the solution for the Blasius function $f(\eta)$, satisfying equation (10), is obtained using the NAG routine D02HAF.

The evolution of the functions $G(\xi,\tau)$ and $\theta(\eta,\tau)$ are separately governed by the partial differential equations (14) and (11), respectively, which are each parabolic and can be integrated numerically using a step-by-step method similar to that described by Merkin [14], provided that the coefficients of the corresponding terms $\partial G/\partial\tau$ and $\partial\theta/\partial\tau$ remain positive throughout the solution domain. This marching method enables the initial state $\theta(\eta,0)=0$, for $\eta\geqslant 0$, at time $\tau=0$ to proceed in time and gives a complete solution for $\tau\leqslant\tau_n^*$, where τ_n^* is the maximum value of τ reached in the forward integrating numerical scheme. The value of τ_n^* will be slightly less than $\tau_p^*=1$, namely within one time increment, and at this time the coefficients of the terms $\partial G/\partial\tau$ and $\partial\theta/\partial\tau$ in equations (14) and (11), respectively, change sign at the outer edge of the thermal boundary-layer. Physically, as well as mathematically, we would expect that $\tau_n^*=1$, since for $\tau<1$ the disturbance from the leading edge has not been felt. The disturbance travels fastest at the outer edge of the boundary-layer and, therefore, it is first encountered at such locations when $\tau=1$. The application of the step-by-step scheme to equation (14), using the known solution for $F(\xi)=f(\eta)|_{\eta=2\xi(\frac{\tau}{\sigma})^{1/2}}$, enables the accurate evolution of the temperature profiles to be determined over a developing inner layer whose width increases with time. If ξ_∞ and η_∞ are interpreted as being finite values of the spatial variables at which the associated boundary conditions are to be applied, then at the exact time $\tilde{\tau}_p=\sigma(\frac{\eta_\infty}{2\xi_\infty})^2$ we must transfer to the step-by-step

scheme applied to equation (11), using the known solution for $f(\eta)$. We again adopt the notation $\tilde{\tau}_n$ to denote the corresponding value of τ which is reached in our numerical techniques.

At the time $\tau = \tau_n^*$ the forward integration approach breaks down and the coefficients of $\partial G/\partial\tau$ and $\partial\theta/\partial\tau$ in the governing equations (14) and (11), respectively, are tending towards negative values as $\eta \to \infty$. Based upon the profile $\theta(\eta, \tau_n^*)$ at this time and the asymptotic steady state profile $\theta_0(\eta)$, defined as the solution of the system of equations (28), we attempt to complete the numerical integration and derive a solution over $\tau_n^* < \tau < \infty$ by adopting a matching approach in section 5.3.

5.1. *Numerical solution for* $0 < \tau \leqslant \tilde{\tau}_n$

In order to evaluate accurately the initial evolution of the non-dimensional fluid temperature θ we apply the direct, forward integration scheme to equation (14), using the known solution for $F(\xi) = f(\eta)|_{\eta=2\xi(\frac{\tau}{\sigma})^{1/2}}$ achieved using the NAG routine D02HAF, and begin the numerical solution at the small time $\tau = \tau_0 > 0$. Thus, the governing equation (14) must be solved subject to the boundary conditions (15) and the initial profile

$$G(\xi, \tau_0) \approx \sum_{n=0}^{N_0-1} \tau_0^{\frac{3}{2}n} \mathcal{G}_n(\xi) \tag{47}$$

expressed as the first N_0 terms from the small time solution (18) of section 3.

The finite spatial domain is divided into N^ξ grid spacings of length $h^\xi = \xi_\infty/N^\xi$ and a variable time step is used, with the time step at the start of the j-th time increment being denoted by $\Delta\tau_j$. We also introduce the notation $G_{i,j}$ to represent the finite-difference approximation to the non-dimensional temperature function G at the point $\xi = (i-1)h^\xi$ for some time $\tau = \tau_j$. The notation F_i is introduced as the known solution for $F(\xi) = f(\eta)|_{\eta=2\xi(\frac{\tau}{\sigma})^{1/2}}$ at the point $\xi = (i-1)h^\xi$ for all times τ. In practice, the NAG routine D02HAF is used to derive a solution for $f(\eta)$ at a specified number of equally spaced grid points over $0 \leqslant \eta \leqslant \eta_\infty$ and $F(\xi)$ can then be determined at any value of ξ within the interval $0 \leqslant \xi \leqslant \xi_\infty$ by linear interpolation, ensuring that this process does not introduce any significant error into the numerical procedure.

Given a complete solution $G_{i,j}$, $i = 1, \ldots, N^\xi + 1$, at time τ_j we require the solution for $G_{i,j+1}$ at the next time $\tau = \tau_{j+1} = \tau_j + \Delta\tau_j$ and adopt the step-by-step finite-difference procedure similar to that described by Merkin [14]. This numerical formulation is very well described by Harris et al. [18] and we will not present it here. The system of linear algebraic equations resulting from the finite-difference approximation to the governing equation (14) is inverted using the Thomas algorithm for tri-diagonal matrices.

To accurately describe the initial evolution, the time increment $\Delta\tau_0$ at time $\tau = \tau_0$ is set to some prescribed small value and subsequently a time step doubling procedure is adopted to reduce the computations at later times.

5.2. *Numerical solution for* $\tilde{\tau}_n < \tau \leqslant \tau_n^*$

As noted earlier, the restrictions to finite-dimensional ξ and η spaces enable us to transfer from the forward integrating solution procedure of section 5.1, in ξ, τ variables, to the same approach in η, τ variables at the precise time $\tilde{\tau}_p = \sigma(\frac{\eta_\infty}{2\xi_\infty})^2$. Based upon the temperature profile at the final time $\tilde{\tau}_n$ reached in the numerical solution of the previous section, we can now continue the step-by-step method, using a technique similar to that described by Merkin [14], towards the time $\tau_p^* = 1$.

The thermal boundary-layer equation (11) is now solved subject to the appropriate boundary conditions (12) and the initial profiles

$$\theta(\eta, \tilde{\tau}_n) = 2\left(\frac{\tilde{\tau}_n}{\sigma}\right)^{1/2} G(\xi, \tilde{\tau}_n)\Big|_{\xi=\frac{1}{2}\eta(\frac{\sigma}{\tilde{\tau}_n})^{1/2}}, \tag{48}$$

where the conditions valid for $\eta \to \infty$ are applied at $\eta = \eta_\infty = 2\xi_\infty(\frac{\tilde{\tau}_n}{\sigma})^{1/2}$. The numerical formulation used in the paper by Harris et al. [18] is employed in a similar manner to that described in section 5.1.

5.3. Numerical solution for $\tau_n^* < \tau < \infty$

At large times the solution for the non-dimensional temperature function $\theta(\eta, \tau)$ is known to approach the steady state solution profile $\theta_0(\eta)$ associated with the uniform heat flux q_w at the plate surface. We must now attempt to characterise the evolution of the profile reached at time τ_n^*, when the numerical techniques of sections 5.1 and 5.2 terminate, towards this final steady state profile.

The matching technique originated by Dennis [15] has been successfully applied by the present authors to some related problems of impulsive changes in uniform surface heat flux or temperature on vertical plates, see Harris et al. [17–19] wherein comprehensive details of this iterative approach are presented. In the finite-difference approximation to equation (11) we replace $\partial\theta/\partial\tau$ by either a backward or forward difference depending on whether the coefficient of $\partial\theta/\partial\tau$ is positive or negative, respectively, to achieve a convergent solution using standard iterative techniques.

6. Results

The NAG routine D02HAF was used to solve both the ordinary differential equation (10), subject to the appropriate boundary conditions (12), and the ordinary differential system (28). In this numerical procedure an absolute error tolerance must be supplied and the upper range of integration must be specified at some finite value instead of infinity. In all the results presented in this paper a tolerance of 10^{-8} and an endpoint of $\eta = 14$ were used as it was found that any further decrease and increase, respectively, of these values did not produce results which showed further significant variation.

In the discussion of the results for the transient temperature field which follows we concentrate on the two cases when the Prandtl number, $\sigma = 0.72$ (air) and 6.7 (water).

6.1. Results for $0 < \tau \leqslant \tau_n^*$

The restriction to a finite-dimensional ξ space was achieved by taking $\xi_\infty = 10$ and 20 for $\sigma = 0.72$ and 6.7, respectively, and thus the precise times at which the transfer to the method of section 5.2 takes place are $\tilde{\tau}_p = 0.35280$ and 0.82075, respectively, taking $\eta_\infty = 14$. The increase in ξ_∞ to $\xi_\infty = 20$ for $\sigma = 6.7$ was made to ensure that $\tilde{\tau}_p < \tau_p^*$ and we transfer to the numerical approach of section 5.2 before the step-by-step method breaks down at $\tau_p^* = 1$. The values of ξ_∞ and η_∞ were separately increased but provided no discernible graphical variation. The initial time τ_0 and first time increment $\Delta\tau_0$ were assigned the values $\tau_0 = 5 \times 10^{-5}$ and $\Delta\tau_0 = 10^{-8}$, respectively, and the initial non-dimensional temperature profile (47) was invoked using $N_0 = 2$ terms in the small time solution. Any modification in the values of these parameters was found to produce a negligible variation in the results achieved. For the Prandtl numbers $\sigma = 0.72$ and 6.7 the time step doubling criterion was successful in steadily increasing the time increments and led to time steps of $\Delta\tau = 4.096 \times 10^{-5}$

and 3.2768×10^{-4} at the times $\tau = \tilde{\tau}_n = 0.35280$ and $\tau = \tilde{\tau}_n = 0.82095$, respectively. The numerical values of $\eta_\infty = 2\xi_\infty(\frac{\tilde{\tau}_n}{\sigma})^{1/2}$ were therefore calculated to be $\eta_\infty = 13.9999$ and $\eta_\infty = 14.0017$ for $\sigma = 0.72$ and 6.7, respectively.

The time τ_n^*, denoting the largest value of τ reached in the step-by-step numerical scheme before $\tau_p^* = 1$ was found to be $\tau_n^* = 0.99996$ and $\tau_n^* = 0.99986$ for $\sigma = 0.72$ and 6.7, respectively.

The most significant source of variation in the solution for the non-dimensional fluid temperature $\theta(\eta, \tau) = 2(\frac{\tau}{\sigma})^{1/2} G(\xi(\eta, \tau), \tau)$ arises by considering changes in the number of grid spaces N^ξ and N^η, applied for the formulation of the step-by-step method in ξ, τ and η, τ variables, respectively. For the case $\sigma = 0.72$, the results obtained for $N^\xi = 100$, 200, 400, 800, 1600, 3200 and 6400 with corresponding values of $h^\xi = 0.1$, 0.05, 0.025, 0.0125, 6.25×10^{-3}, 3.125×10^{-3} and 1.5625×10^{-3}, respectively, are compared against the small time solution of section 3, employing 1, 3, 9 and 11 terms, in *table I*. At each time instant considered in this table, the highest-order small time solution displayed is accurate to seven decimal places. As the number of grid spacings employed in the numerical procedure is increased from $N = 100$ to 6400 the solutions obtained for the initial development of the non-dimensional plate temperature are observed to converge towards the most accurate small time solution, although the improvement in accuracy is less significant beyond the refinement to the $N = 1600$ grid spacings. The efficiency of this numerical procedure enables solutions to be achieved rapidly using $h^\xi = 6.25 \times 10^{-3}$ and therefore this value has been used in all the results presented in this paper, so that $N^\xi = 1600$ and 3200 for $\sigma = 0.72$ and 6.7, respectively. Furthermore, the number of spatial grid points and final time increment at $\tau = \tilde{\tau}_n$ were continued to the method described in section 5.2 for $\tilde{\tau}_n < \tau \leqslant \tau_n^*$, so that $N^\eta = 1600$ and $h^\eta = \frac{\eta_\infty}{N^\eta} = 8.75 \times 10^{-3}$.

Figure 1 shows the variation of the temperature profiles $\theta(\eta, \tau)$ at various times τ calculated for $\sigma = 0.72$ and 6.7. The steady state solution as predicted by equation (28) is also included in this figure. We see that the non-dimensional temperature profiles evolve from $\tau = 0$ towards the large time steady state solution although initially the effects of the imposed surface heat flux at the plate are not felt near the outer edge of the velocity boundary-layer. As time progresses towards $\tau = \tau_n^*$ the effect of the impulsive change in the surface conditions penetrate further into the steady velocity boundary-layer. In the final decay to the steady state profiles, the departures from the steady state solution are again concentrated near to the plate, providing justification for the inner solution formulation used in the large time solution of section 4.

The evolution of the non-dimensional plate surface temperature with time τ is presented in *figure 2* and this numerical, transient solution is shown to develop closely following the small time solution and is graphically almost identical when $\tau < 1.65$ and $\tau < 3.15$ for $\sigma = 0.72$ and 6.7, respectively, if 5 or more terms are employed in this small τ expansion. It is important to note that, although the small time solution provides good agreement with the full numerical solution for the surface temperature over a range of values of τ greater than unity, clearly the agreement between the two techniques is not as good in the outer regions of the boundary-layer, where the effect of the leading edge disturbance has been felt. This disturbance then diffuses towards the plate and hence produces the discrepancy between the solutions obtained from the two techniques for $\tau > 1$. As the number of terms in the small time solution is increased from 1 to 5, significant improvements in the upper limit of the range of its validity are observed. However, the inclusion of any more terms in the series provides no significant improvement in either the accuracy of the approximation or the upper bound of the range of validity. This graphical observation is confirmed by the results displayed in *table I*. The first 15 values of the terms $\mathcal{G}_n(0)$ in the small time solution (18) at $\xi = 0$, as determined using the numerical procedure described in section 3, are presented in *table II* for $\sigma = 0.72$ and have been determined also for $\sigma = 6.7$ to around the $n = 20$ term. As the numerical solution for the non-dimensional plate temperature begins to deviate from the small time solution, this truncated series approximation becomes invalid.

To further demonstrate the validity of the small time solution, the predicted profiles of the non-dimensional temperature $\theta(\eta, \tau)$ using 7 terms in the series approximation (18) have been included in *figure 1*, represented by dotted lines, at the same time instants used for the numerical solution profiles. Only the profiles up to the times $\tau < 1.65$ and $\tau < 3.15$ for $\sigma = 0.72$ and 6.7, respectively, have been presented since the small time solution for the plate temperature is known to be invalid beyond these times, as observed in *figure 2*. The small time solutions are seen to provide an excellent approximation to the numerical temperature profiles until times approaching the upper bound of the range of validity of the solutions at the plate. At such times the small

Table I. Comparison of the small time solution for the non-dimensional plate temperature, evaluated using different numbers of terms in expression (18), with the step-by-step numerical solutions, developed in sections 5.1 and 5.2, using $N = N^{\xi} = N^{\eta}$ grid spacings, when $\sigma = 0.72$.

Numerical	Non-dimensional time, τ				
solution	0.01	0.1	0.2	0.5	0.9
$N = 100$	0.1328172	0.4201414	0.5945465	0.9430043	1.2736717
$N = 200$	0.1329409	0.4205354	0.5951046	0.9438109	1.2744106
$N = 400$	0.1329719	0.4206339	0.5952442	0.9440126	1.2745952
$N = 800$	0.1329796	0.4206585	0.5952791	0.9440630	1.2746413
$N = 1600$	0.1329816	0.4206647	0.5952878	0.9440756	1.2746529
$N = 3200$	0.1329820	0.4206662	0.5952890	0.9440787	1.2746558
$N = 6400$	0.1329822	0.4206666	0.5952905	0.9440795	1.2746565
Small time solution					
1 Term	0.1329808	0.4206662	0.5952845	0.9439190	1.2732402
3 Terms	0.1329822	0.4206667	0.5952907	0.9440788	1.2746012
9 Terms				0.9440798	1.2746566
11 Terms					1.2746567

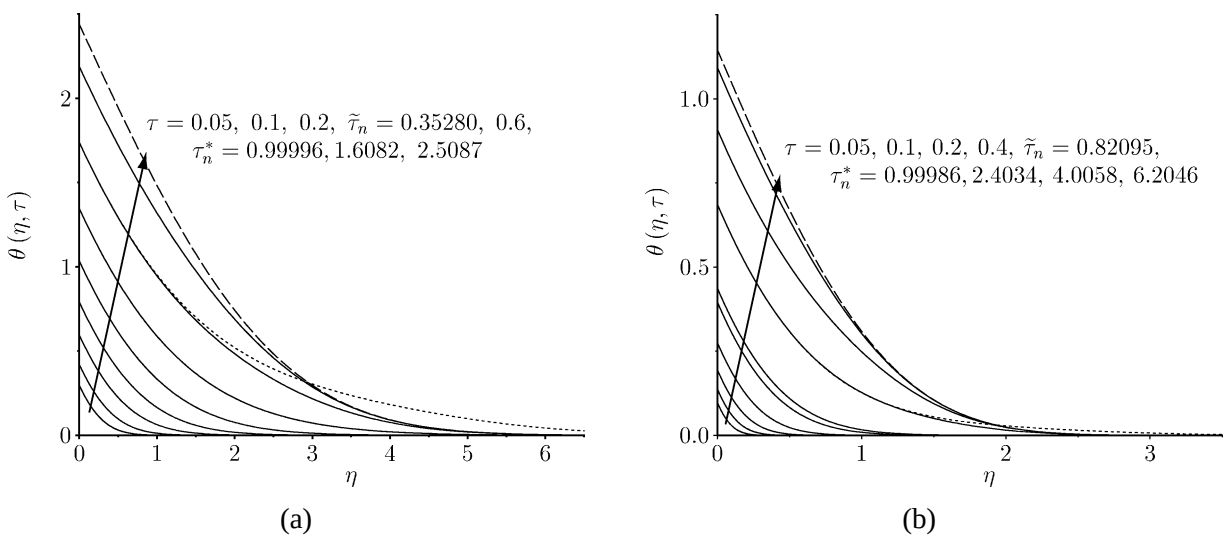

Figure 1. Variation of the non-dimensional temperature function $\theta(\eta, \tau)$ as a function of η, shown at various values of τ during the evolution from the initial unsteady state at $\tau = 0$ to the large time solution valid as $\tau \to \infty$. The numerical solutions are indicated by the solid lines, the small time solutions (18) are indicated by the dotted lines and the large time steady state profile, satisfying the ordinary differential system (28), is indicated by the broken line: (a) $\sigma = 0.72$; (b) $\sigma = 6.7$.

Table II. The first 15 values of the terms $\mathcal{G}_n(0)$ in the small time solution (18) at $\xi = 0$, as determined using the computer expansion procedure described in section 3, when $\sigma = 0.72$.

n	$\mathcal{G}_n(0)$
0	$0.564190 = \pi^{-\frac{1}{2}}$
1	6.11458×10^{-3}
2	7.18580×10^{-4}
3	1.36303×10^{-4}
4	3.40343×10^{-5}
5	1.02551×10^{-5}
6	3.54558×10^{-6}
7	1.36126×10^{-6}
8	5.67566×10^{-7}
9	2.52936×10^{-7}
10	1.19086×10^{-7}
11	5.87196×10^{-8}
12	3.01200×10^{-8}
13	1.59872×10^{-8}
14	8.74409×10^{-9}

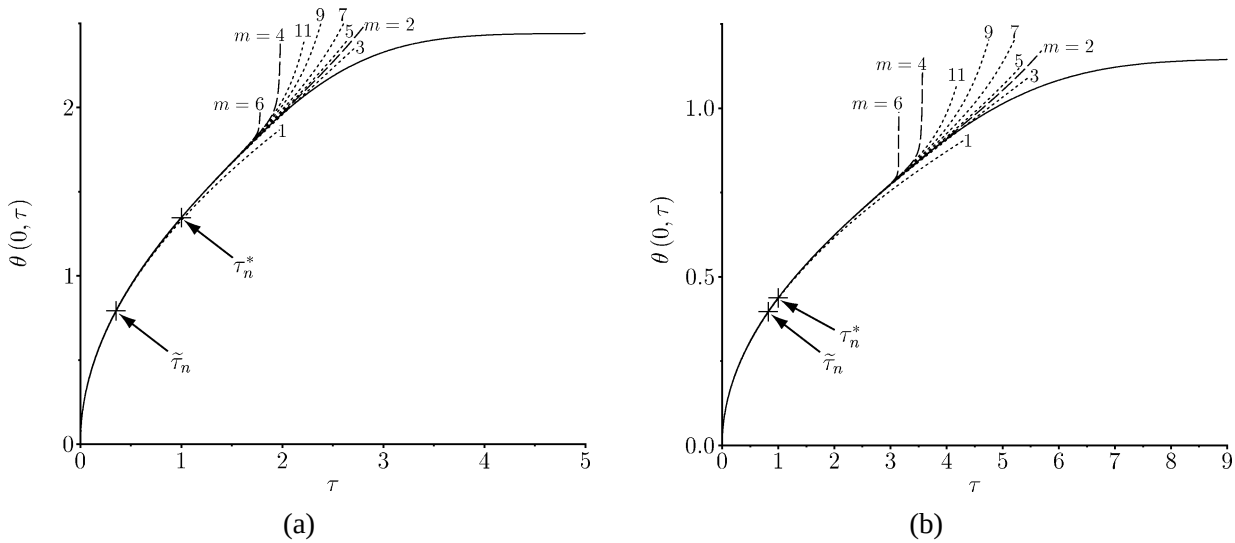

Figure 2. Variation of the non-dimensional plate temperature $\theta(0,\tau)$ as a function of τ determined numerically (solid line), using the 1, 3, 5, 7, 9 and 11 term small time solutions (18) (dotted lines) and using the Shanks solutions (50) for $m = 2$, 4 and 6 (broken lines), where the transitions between the solution methods of sections 5.1 and 5.2 and sections 5.2 and 5.3 occur at the indicated times $\tilde{\tau}_n$ and τ_n^*, respectively: (a) $\sigma = 0.72$; (b) $\sigma = 6.7$.

time approximation breaks down with increasing distance from the plate, possibly due to increasing numerical inaccuracies developed in the calculation of the terms containing $A_{n,3k}\xi^{3k}$ in the general form (26).

In order to attempt to extend the upper range of the validity of the small time solution developed in section 3 and accelerate the convergence of the series (18) at $\xi = 0$, the transformation devised by Shanks [13] is now implemented. Thus, instead of the functions

$$G^{(r)}(0,\tau) = \sum_{n=0}^{r} \tau^{\frac{3}{2}n} \mathcal{G}_n(0) \tag{49}$$

for $r = 0, 1, 2, \ldots, m$, which provide a set of partial sums leading to the $(m+1)$-term small time solution $G^{(m)}(0, \tau)$, we consider the sequence

$$e_i^k = \frac{e_{i+1}^{k-1} e_{i-1}^{k-1} - (e_i^{k-1})^2}{e_{i+1}^{k-1} + e_{i-1}^{k-1} - 2e_i^{k-1}} \tag{50}$$

for $i = k, k+1, \ldots, m-k$ and $k = 1, 2, \ldots, \frac{m}{2}$ if m is even or $k = 1, 2, \ldots, \frac{m-1}{2}$ if m is odd. Here $e_i^0 = G^{(i)}(0, \tau)$ for $i = 0, 1, 2, \ldots, m$.

The small time solutions for the non-dimensional wall temperature function $G(0, \tau)$ derived from applying the Shanks transformation (50) for $m = 2$, 4 and 6 to the partial sums (49) leading to the 3, 5 and 7 term solutions, have been transformed into $\theta(0, \tau) = 2(\frac{\tau}{\sigma})^{1/2} G(0, \tau)$ and they are included in *figure 2*. From this figure it can be seen that only for $m = 2$ does the Shanks method accelerate slightly the convergence of the small time solution (18) at $\xi = 0$, whilst for $m = 4$, and beyond, there is no significant improvement in convergence. This observation is in accordance with results obtained by Lesnic et al. [24] for a related study in a porous medium. Furthermore, the use of the Shanks method is seen not to extend the range of validity of the small time solution. This may have been expected due to the singular nature of the governing partial differential equation (11), which clearly shows that information is being transferred both in the positive and negative τ directions.

6.2. Results for $\tau_n^* < \tau < \infty$

The matching technique originated by Dennis [15] was applied in order to predict the evolution of the known profile of the non-dimensional temperature reached at the termination of the forward integrating approach of sections 5.1 and 5.2 towards the ultimate, large time steady state profiles. The spatial grid size specified at $\tau = \tau_n^*$, from the termination of the forward integration approach, was continued here, whilst maintaining the value $\eta_\infty \approx 14$ which has been shown to be valid for $\tau \leqslant \tau_n^*$. The restriction to a finite temporal domain requires that the final steady state profiles must be enforced at the finite value $\tau = \tau_\infty$, corresponding to $\tau \to \infty$. The solution profiles for the non-dimensional temperature have been observed to smoothly approach their steady state solutions when τ_∞ is imposed at $\tau_\infty = 5$ and 9 for $\sigma = 0.72$ and 6.7, respectively, with no significant improvement in accuracy when τ_∞ is extended beyond these values.

An investigation of the effect of the spatial and temporal grid sizes $\tilde{h} = \frac{\eta_\infty}{n}$ and $\tilde{k} = \frac{\tau_\infty - \tau_n^*}{m}$ using n and m grid spacings, respectively, on the solution for the non-dimensional temperature was performed. It is common in problems of this type to require that $\tilde{h} \approx \tilde{k}$, as observed in Harris et al. [18–20], but no such restriction was needed here. The case $\tilde{h} = 0.0175$ and $\tilde{k} = 0.01167$, corresponding to $n = 800$ and $m = 342$ and 684 for $\sigma = 0.72$ and 6.7, respectively, were chosen for the presentation of results within this paper and no significant deviation from the associated temperature profiles was observed with any further refinement in these discretisations. It should be noted that a significant increase in computational time was required for the production of solutions on the $n = 1600$ spatial grid and the solutions obtained using $n = 800$ and the same temporal grid were in agreement to at least 7 significant figures for times close to τ_n^* and 5 significant figures in the approach to τ_∞.

The convergence of the iterative scheme is described by the approach of the average absolute error over the solution domain to a specified error tolerance. Due to the slow convergence of this numerical procedure, the error tolerance is made small, namely 5×10^{-10}, and the solutions thereby produced are again correct to at least 7 significant figures for times close to τ_n^* and 4 significant figures in the approach to τ_∞, for the parameters under investigation.

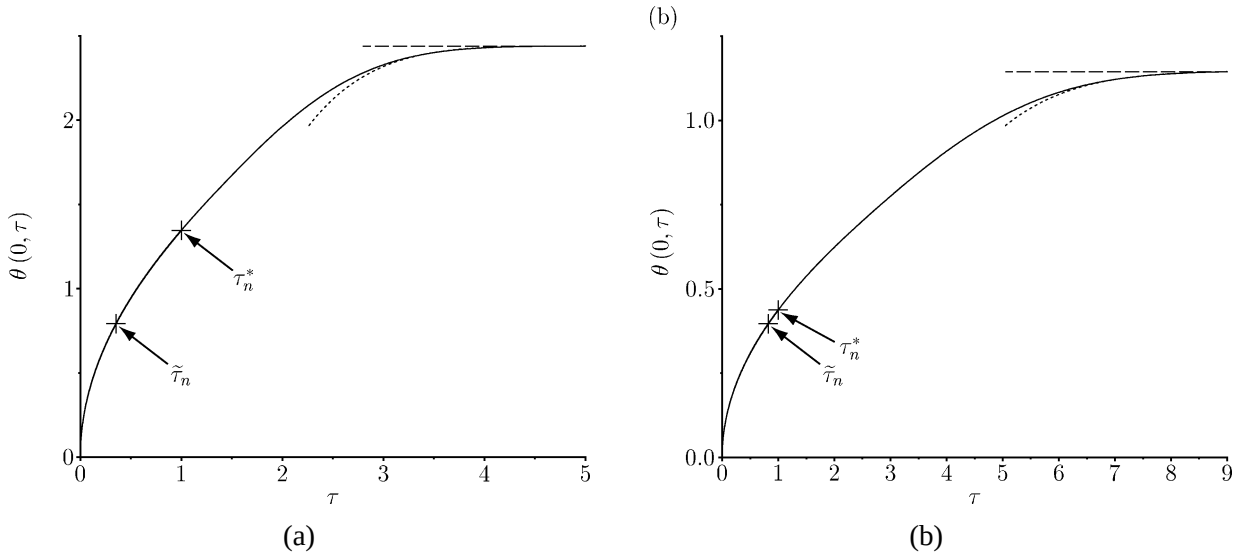

Figure 3. Variation of the non-dimensional plate temperature $\theta(0,\tau)$ as a function of τ determined numerically (solid line), the steady state solution valid as $\tau \to \infty$ (broken line) and the large time approximate solution (51) using an appropriate value of K (dotted line), where the transitions between the solution methods of sections 5.1 and 5.2 and sections 5.2 and 5.3 occur at the indicated times $\tilde{\tau}_n$ and τ_n^*, respectively: (a) $K = 3.97$ for $\sigma = 0.72$; (b) $K = 8.42$ for $\sigma = 6.7$.

The transient development of the non-dimensional temperature at the plate determined using the matching method, continuing from the solutions described in section 6.1, has been included in *figures 2* and *3*. Some additional profiles of the non-dimensional temperature have also been presented in *figure 1* beyond the time τ_n^*.

The form of the large time solution profiles shown in equation (29), with $\theta_0(\eta)$ defined as the solution of the system (28) and $\theta_1(\eta,\tau)$ given by expression (46), indicates that the behaviour of the non-dimensional temperature at the plate surface behaves like

$$\theta(0,\tau) = \theta_0(0) - K\tau^{c_1}\exp\left(-\frac{1}{3}\frac{s_1^3\alpha^2}{\sigma}\tau^3\right) \tag{51}$$

as $\tau \to \infty$, where $s_1 = 1.018793$ from section 4, c_1 is defined in equation (45) and $K = C_0\mathrm{Ai}(-s_1)$ is a constant to be determined. Using the NAG routine D02HAF, the system (28) has been solved for $\sigma = 0.72$ and 6.7 to give $\theta_0(0) = 2.4397885$ and 1.1458402, respectively. The particular choices $K = 3.97$ and 8.42, for $\sigma = 0.72$ and 6.7, respectively, have been used to provide an approximation to the transient behaviour of the non-dimensional wall temperature for large values of τ in *figure 3*. This figure demonstrates that, for the chosen values of K, the large time approximation (51) for $\theta(0,\tau)$ is graphically indistinguishable from the numerical solution for the plate temperature developed in section 5 if $\tau \gtrsim 3.3$ and 6.7 when $\sigma = 0.72$ and 6.7, respectively, and provides a better prediction of the approach to steady state than given by the constant value $\theta_0(0)$.

7. Conclusions

The transient forced convection heat transfer from a fixed, flat plate situated in a fluid of initially uniform temperature and constant far-field velocity, which develops in response to the sudden initiation of a constant surface heating rate, has been analysed thoroughly. This type of situation occurs frequently in practice but, of course, the present approach is an idealisation with an instantaneous change in the boundary condition at the

plate surface. The analytical solution for the fluid temperature using the first three terms in a series expansion, which is valid for small times, has been extended through a numerical procedure suggested by van Dyke [10] and this approach provides fluid temperature profiles which are both more accurate and valid up to a later instant in time. The transformation introduced by Shanks [13] has been implemented in order to attempt to improve upon the predictive capabilities of the small time approximation but was found to be unsuccessful in extending the upper bound of the range of its validity.

The results obtained from the small time approximations do not enable a transition from the initial unsteady state to the ultimate steady state solution to be achieved and therefore an accurate numerical solution of the equations governing the development of the thermal boundary-layer was performed. A sequence of numerical procedures have been presented for the whole transient from $\tau = 0$ to the steady state $\tau \to \infty$. These procedures consist of a modification of the forward integration method proposed by Merkin [14] in combination with a finite-difference method similar to that devised by Dennis [15], beyond times at which the initial marching procedure is no longer well posed, and the results have been validated against the small time solution. The primary source of variation in the numerical solutions obtained arises due to variations in the spatial and temporal discretisations of the solution domain and these effects have been analysed in detail to ensure the accuracy of the results presented. It has been shown that the small time transient is initially confined within a region close to the plate surface but, as time progresses, diffusion effects eventually modify the solution at a greater distance from the plate. A large time solution has also been presented and shown to provide an approximation to the approach of the plate temperature to its large time steady state value. In this approach to the large time steady state solution, the deviation from the steady state profile is again concentrated near to the plate.

The effect of the value of the Prandtl number, σ, on the temperature field has been investigated through a thorough study of the representative cases $\sigma = 0.72$ (air) and 6.7 (water). As expected, an increase in the value of the Prandtl number, which occurs in the governing equation (11) in the coefficient $1/\sigma$ of the thermal diffusion term, results in an increase in the time taken to reach the steady state solution (see *figures 2* and *3*), a decrease in the thermal boundary-layer thickness (see *figure 1*) and, therefore, a decrease in the steady state plate temperature.

Finally, it should be noted that the method described in the present paper applies equally as well when the heat flux is suddenly changed from a non-zero value to a different value, and we hope to report results on this problem in the near future.

Acknowledgements

The authors are grateful to the three referees for their very constructive comments. Also, D.B. Ingham and I. Pop would like to thank The Royal Society for some financial support.

References

[1] Riley N., Unsteady laminar boundary layers, SIAM Rev. 17 (1975) 274–297.
[2] Riley N., Unsteady viscous flows, Sci. Progress Oxford 74 (1990) 361–377.
[3] Shen S.-F., Unsteady separation according to the boundary-layer equation, Adv. Appl. Mech. 18 (1978) 177–220.
[4] Telionis D.R., Review – Unsteady boundary-layers, separated and attached, J. Fluids Eng. 101 (1979) 29–43.
[5] Telionis D.R., Unsteady Viscous Flows, Springer, New York, 1981.
[6] Pop I., Transient heat transfer in boundary-layer flows, in: Padet J., Arinç F. (Eds.), Proc. Int. Symposium on Transient Convective Heat Transfer, Begell House, New York, 1997.
[7] Riley N., Unsteady heat transfer for flow over a flat plate, J. Fluid Mech. 17 (1963) 97–104.

[8] Chao B.T., Cheema L.S., Unsteady heat transfer in laminar boundary-layer over a flat plate, Int. J. Heat Mass Tran. 11 (1968) 1311–1324.
[9] Dennis S.C.R., Unsteady heat transfer for boundary-layer flow over a flat plate, in: Recent Research on Unsteady Boundary Layers, Volume 1, IUTAM Symposium 1971, Laval Univ. Press, Quebec, 1972, pp. 379–403.
[10] Van Dyke M., Computer extension of perturbation series in fluid mechanics, SIAM J. Appl. Math. 28 (1975) 720–733.
[11] Watkins C.B., Heat transfer in the laminar boundary-layer over an impulsively started flat plate, J. Heat Trans-T. ASME 97 (1975) 482–484.
[12] Jeng D.R., Lee M.H., De Witt K.J., The final approach to steady state in nonsteady stagnation point heat transfer, J. Eng. Math. 10 (1976) 173–185.
[13] Shanks D., Non-linear transformations of divergent and slowly convergent sequences, J. Math. Phys. 34 (1955) 1–42.
[14] Merkin J.H, Free convection with blowing and suction, Int. J. Heat Mass Tran. 15 (1972) 989–999.
[15] Dennis S.C.R., The motion of a viscous fluid past an impulsively started semi-infinite flat plate, J. Inst. Math. Appl. 10 (1972) 105–117.
[16] Walker J.D.A., Dennis S.C.R., The boundary layer in a shock tube, J. Fluid Mech. 56 (1972) 19–47.
[17] Harris S.D., Ingham D.B., Pop I., Transient free convection on a vertical plate subjected to a change in surface heat flux in porous media, Fluid Dyn. Res. 18 (1996) 313–324.
[18] Harris S.D., Ingham D.B., Pop I., Free convection from a vertical plate in a porous medium subjected to a sudden change in surface heat flux, Transport Porous Med. 26 (1997) 207–226.
[19] Harris S.D., Ingham D.B., Pop I., Free convection from a vertical plate in a porous media subjected to a sudden change in surface temperature, Int. Commun. Heat Mass 24 (1997) 543–552.
[20] Harris S.D., Elliott L., Ingham D.B., Pop I., Transient free convection flow past a vertical flat plate subjected to a sudden change in surface temperature, Int. J. Heat Mass Tran. 41 (1998) 357–372.
[21] Rosenhead L., Laminar Boundary Layers, Oxford University Press, Oxford, 1963.
[22] Stewartson K., On the impulsive motion of a flat plate in a viscous fluid, Q. J. Mech. Appl. Math. 4 (1951) 182–198.
[23] Bender C.M., Orszag S.A., Advanced Mathematical Methods for Scientists and Engineers, McGraw-Hill, Singapore, 1978.
[24] Lesnic D., Ingham D.B., Pop I., Free convection boundary-layer flow along a vertical surface in a porous medium with Newtonian heating, Int. J. Heat Mass Tran. 42 (1999) 2621–2627.